Spring 2022

Simulation, Optimization, and Economic Assessment of Pelamis Wave Energy Converter

Hana Ghaneei
Northern Illinois University, z1939548@students.niu.edu

Mohammadreza Mahmoudi
Northern Illinois University

WECs in AQWA

Hana Ghaneei

Mohammadreza Mahmoudi

Ghaneei and Mahmoudi simulate the dynamic behaviour of Pelamis in AQWA software.

Who should read this paper?

This paper aims to bring a better understanding of Pelamis wave energy converter (WEC) operation for those who want to make geometric changes in Pelamis and re-examine its parametric under various marine conditions. Scholars who study hydrodynamic simulations of Pelamis or a horizontal semi-immersed cylinder using numerical methods such as finite volume, finite element, and smooth-particle hydrodynamics will be interested in this paper.

Why is it important?

In designing WECs, an accurate prediction of complex wave-structure interactions is a crucial consideration because they should operate optimally under different wave conditions. It is obvious that the experimental offshore studies are costly and time-consuming processes, and theoretical methods are based on approximations which are so restrictive they limit the simulation accuracy of WECs. In contrast, computational fluid dynamics methods can be appropriate methods. In this study, which is among the first attempts to use a boundary element – that is, a numerical computational method – Pelamis was simulated in different marine conditions to assess its optimal operation.

Marine energy resources are most predictable among all renewable energies. This characteristic makes it valuable to energy markets. Hence, investment in marine energy converter technologies has considerably increased. The Pelamis was selected because, compared to other WECs, it has several advantages such as high stability and adaption to harsh environments.

About the authors

Hana Ghaneei is a master's student in industrial engineering in Northern Illinois University, U.S. She holds a master's in civil engineering, offshore structures from Science and Research branch of Azad University, Tehran, Iran. Her research interests include renewable energy, wave energy converters, and optimization.

Mohammadreza Mahmoudi is a PhD candidate at Northern Illinois University. His research interests include financial economics, computational economics, applied econometrics, and optimization.

SIMULATION, OPTIMIZATION, AND ECONOMIC ASSESSMENT OF PELAMIS WAVE ENERGY CONVERTER

Hana Ghaneei[1] and Mohammadreza Mahmoudi[2]
[1]Department of Industrial and System Engineering, Northern Illinois University, Dekalb, U.S.; z1939548@students.niu.edu
[2]Department of Economics, Northern Illinois University, Dekalb, U.S.; mmahmoudi@niu.edu

ABSTRACT

Wave energy and power is accessible on almost any body of water. One of the most widely known floating structures to generate renewable energy from the seas and the ocean is wave energy converter Pelamis. In this study, an attempt was made to simulate the dynamic behaviour of Pelamis P2 in the software AQWA under the influence of a nonlinear second-order Stokes wave. Pelamis P2 was simulated in different marine conditions including different water depths, wave heights, periods, and angles to assess its optimal operation. With the results in mind, it can be argued that with an increase in water depth, the intensity of the forces created in the joints decrease. This kind of converter shows better efficiency with lower wave heights, while with a rise in the wave periods, the absorbed energy amounts fall. In the modelling, the best collision angle for the waves is when the Pelamis is in the same direction with the waves. The dynamic behaviour of the converter under the effect of irregular waves was surveyed; it shows a better performance under irregular waves compared with regular waves.

KEYWORDS

Pelamis; Wave energy converter; Boundary element; Hydrodynamic analysis; Wave energy; AQWA

INTRODUCTION

The Earth's average surface temperature has increased about 1.18°C since the late 19th century. The main causes of this change are rise of carbon dioxide (CO_2) levels in the atmosphere and other human activities [Gaffney and Steffen, 2017]. Based on NASA's Global Climate Change website, CO_2 is the most effective gas at trapping heat (greenhouse effect) and the largest source of it is burning fossil fuels. Atmospheric concentrations of CO_2 have been increased by human activity more than 48% in comparison with pre-industrial levels. This is more than what happened naturally over a 20,000-year period (from the Last Glacial Maximum to 1850, from 185 ppm to 280 ppm). These harmful and long-standing effects of fossil fuel on the Earth indicate the importance of the development of a number of alternative sources of energy that are renewable and non-polluting. Renewable energy sources include biomass, hydropower, geothermal, wind, wave, and solar energy, whose sources are naturally replenishing. Based on data provided by the U.S. Energy Information Administration, renewable energy accounted for about 12% of total primary energy consumption in the United States in 2020. It also emphasized that renewable energy can decrease energy imports and reduce fossil fuel use. Therefore, it plays an important role in U.S. energy security and in reducing greenhouse gas emissions. Due to the vital role of renewable energies like wave energy in the environment and economy of the U.S., government should invest more money to develop these new energy resources than before.

Moreover, other countries like Canada and Iran, whose economies depend on oil revenues, should consider new sources of energy in order to reduce their budget dependency on oil price fluctuation and achieve sustainable economic development in the long-run [Mahmoudi and Ghaneei, 2022; Mahmoudi, 2021]. These new sources of energy play a pivotal role in the global economy more and more, especially since the COVID-19 pandemic [Mahmoudi, 2022]. It is worth bearing in mind that the first step to developing renewable energy is conducting feasibility studies. Since feasibility studies analyze a project financially and economically, they help us gain a comprehensive perspective. There are a limited number of feasibility studies in the case of United States that provide an assessment of renewable energies. Therefore, there is an obvious need for a well-designed feasibility study. The next major steps are simulation and optimization of energy converters.

Wave energy has long been considered as one of the most promising renewable energy sources and wave energy converters are devices to catch this kind of energy. In the design of wave energy converters (WEC), an accurate prediction of complex wave-structure interactions is a crucial consideration because they should operate optimally under different wave conditions. It is obvious that the experimental offshore studies are costly and time consuming processes, and theoretical methods are based on approximations which are so restrictive that they limit the simulation accuracy of WECs. Wave diffraction and radiation effects are taken into account in theoretical methods while viscous effects and nonlinear effects

are neglected. There is general agreement that computational fluid dynamics (CFD) methods – which not only consider all nonlinear wave diffraction, radiation, and viscous effects but are also qualified in simulation problems which are difficult or impossible to carry out in experimental studies – can be a suitable method for evaluating nonlinear wave force on a body.

The Pelamis WEC is a floating offshore device composed of multiple cylindrical sections linked by hinged joints that converts ocean wave energy into electrical energy. Compared with other WECs, the Pelamis has several advantages such as high stability and adaption to harsh environments. In addition to efficiently generating electricity from offshore waves, the Pelamis WEC is environmentally friendly. Pelamis was discovered to have notably lower environmental impact compared to conventional fossil-fuelled power generation [Thomson et al., 2019]. Therefore, to achieve the main goal of this paper, which is a comprehensive understanding of the optimized function of Pelamis, it is crucial to analyze the Pelamis's performance in a wide range of conditions through dynamic behaviour simulation.

In the present study, using the numerical boundary element method, an attempt has been made to simulate the dynamic behaviour of Pelamis P2 (the P2 is the second-generation design of Pelamis WEC) in the software ANSYS AQWA under the influence of the nonlinear second-order Stokes wave and Joint North Sea Wave Project (JONSWAP) wave spectrum. Firstly, in order to verify the simulations and results, a fixed semi-immersed horizontal cylinder is simulated and the results have been compared with experimental results, the linear potential theory results, and finite volume results which were carried out using OpenFOAM by Loh et al. [2018]. Secondly, P2 Pelamis was simulated in different marine conditions including different water depths, wave heights, periods, and angles.

In recent years, there have been many studies specifically with Pelamis. Dalton et al. [2010] conducted the feasibility study of Pelamis wave energy converter using wave energy data from different locations throughout the world. They created an Excel model which estimated the annual energy output of Pelamis for each location based on wave height and period and they reported financial costs based on input parameters. Westphalen et al. [2010] used four methods for the hydrodynamic simulation of the Pelamis wave energy converter. These methods were the Smoothed Particle Hydrodynamics, a Cartesian Cut Cell method, a Finite Volume method, and a control volume based Finite Element approach. Liu et al. [2011] computed wave forces and floating body motion by a 3D time-domain Green function method. Both infinite and finite water depths cases were investigated in their study. Ganesan and Sen [2015], using time-domain 3D Rankine panel method, studied steep nonlinear waves interacting with a fixed structure. Li and Lin [2012] studied a stationary floating structure under regular and irregular waves in different water depths, wave heights, and periods and calculated nonlinear wave-body interactions in a 2D numerical wave tank. Then they compared their results with experimental and theoretical results [Yemm et al., 2012] by reviewing the progress of Pelamis from its

origin to its commercial deployment which emphasized that Pelamis is a unique wave energy converter device that can convert energy in reliable and affordable ways. Liu et al. [2016] tried to develop a boundary element numerical method for computing the diffraction and radiation of waves that collide with a horizontal long cylindrical structure. Bruinsma et al. [2018] used a fully nonlinear wave tank to simulate complicated wave-structure interactions of moored floating structures. The tank was based on the Navier-Stokes/6-degrees of freedom (DOF) solver and inter-DyMfoam provided by the open-source CFD-toolbox OpenFOAM. Loh et al. [2018] simulated a semi-immersed horizontal cylinder under different types of wave conditions using OpenFOAM which uses the finite volume method for solving the discretized Navier-Stokes equations. After computing horizontal and vertical forces, they compared those results with linear wave theory and experimental data which was carried out by Martin and Dixon [1983].

THEORETICAL ANALYSIS

AQWA is a set of engineering tools used for examining the effects of wave, wind, and current on fixed offshore and floating structures, as well as other ocean structures like compliant towers, conventional tension leg platform, floating production storage and offloading vessels, semi-submersible structures, ships, WECs, and breakwaters. The following actions were taken to perform a hydrodynamic analysis in AQWA:

1. Create a hydrodynamic analysis system.
2. Attach geometry: there are no geometry creation tools in the AQWA application so the geometry must be attached to the hydrodynamic system. The geometry can be defined from either of the following sources: Workbench using DesignModeler or a CAD system supported by Workbench.
    a. General Modelling Requirements: it should be noted that there are some general modelling requirements that should be considered during geometric modelling.
    b. Configuring the Geometry: it is important that the correct water depth is specified, especially with shallow water conditions, since the seabed acts as a boundary condition to the diffraction analysis.
3. Define parts behaviour: each part will be assigned a structure number for the analysis; the parts can be included or excluded from the analysis.
4. Structure connection points: the connections object helps to create connections between structures or between structures and the environment; the available connections are Cables, Catenary Data, Connection Stiffness, Fenders, Joints.
5. Mesh: the mesh is automatically generated on the bodies of the model; its density is based on the defeaturing tolerance and maximum element size parameters.
6. Establish analysis settings which include Time Response Options, Start Time, Finish Time, Time Step, Number of Steps, etc.

Governing Equations for Fluid Flow

The flow was considered to be irrotational and the fluid was inviscid and incompressible; therefore, the velocity was defined by the

gradient of the potential scalar field or velocity potential Φ :

$$\vec{v} = \nabla\Phi \tag{1}$$

Under these assumptions, the governing equation for fluid flow is the Laplace's equation:

$$\nabla^2\Phi(x\ y\ z\ t) = 0 \tag{2}$$

Based on superposition principle:

$$\Phi(x\ y\ z\ t) = \Phi_s + \Phi_r \tag{3}$$

where Φ is the total velocity potential, Φ_s is the scattering potential, and Φ_r is the radiation potential.

Wave Theory

There are various wave theories available in AQWA which can be chosen to generate waves. Maintained as valid on the part of numerous theories of periodic water wave in Huntley [1977], the Stokes second-order wave theory is the most appropriate for the wave parameters adopted on the present research.

Second-order Stokes Wave Theory

Stokes in 1847, using the perturbation technique, presented a finite domain wave theory for solving the problem of wave boundary values, where all wave characteristics (velocity potential, velocity, surface profile, etc.) are formulated in terms of power series expressions at higher consecutive degrees of wave steepness (H/L). In this theory, it is assumed that the wave height is small when compared to the water depth. Second-order Stokes wave theory is more common in engineering applications and, for offshore designs, the fifth-order Stokes wave theory is more practical to use. Pelamis is used in deep and relatively deep waters (usually more than 50 m); therefore, the second-order Stokes wave theory has been used to simulate Pelamis WEC under wave action.

According to this theory, the wave surface elevation is obtained by the following equation:

$$\eta = \frac{H}{2}\cos(kx - \omega t) + \frac{\pi H}{8}\left(\frac{H}{L}\right)\frac{\cosh kd\,(2+\cosh 2kd)}{\sinh^3 kd}\cos 2(kx - \omega t) \tag{4}$$

where k is the wave number and ω is the angular frequency which is a function of the wave length λ and the period T. They are determined by the following equations:

$$k = \frac{2\pi}{\lambda} \tag{5}$$

$$\omega = \frac{2\pi}{T} \tag{6}$$

Where the horizontal and vertical components of the velocity of water particles represented by u and v, respectively, are calculated by the following equations:

$$u = \frac{\omega H}{2}\frac{\cosh ky}{\sinh kd}\cos(kx - \omega t) + \frac{3(\pi H)^2}{4TL}\frac{\cosh 2ky}{\sinh^4 kd}\cos 2(kx - \omega t) \tag{7}$$

$$v = \frac{\omega H}{2}\frac{\sinh ky}{\sinh kd}\sin(kx - \omega t) + \frac{3(\pi H)^2}{4TL}\frac{\sinh 2ky}{\sinh^4 kd}\sin 2(kx - \omega t) \tag{8}$$

In the above equations, $k = \frac{2\pi}{\lambda}$ and ω are the wave number and angular frequency of the

wave, respectively, and λ is the wave length which are related by the following equation:

$$\omega^2 = gk\tanh(kd) \quad (9)$$

In the above equation, g is the gravitational acceleration.

It should be noted that, if the wave period is known, the angular frequency can be calculated by $\omega = 2\pi/T$. Then, the wave number can be determined using the latter equation. To do this, the equation is rewritten as follows:

$$k = \frac{\omega^2}{g\tanh(kd)} \quad (10)$$

Now by replacing ω and assuming an initial value for kd (for example, 1) the equation will be solved and value of k will be obtained. This will be repeated for different values of kd until the value of k obtained from the left side of the equation is the same as the value of k assumed to the right of the equation. Gauge pressure (the difference between actual pressure and atmospheric pressure) at any point with the coordinate (x,y) at the time t, which is the sum of dynamic pressure induced by the wave and the hydrostatic pressure, is obtained by:

$$P = \rho g(d-y) + \frac{\rho gH}{2}\frac{\cosh ky}{\cosh kd}\cos(kx-\omega t) + \frac{3\pi\rho gH^2}{4L\sinh 2kd}\left[\frac{\cosh 2ky}{\sinh^2 kd} - \frac{1}{3}\right]\cos 2(kx-\omega t) - \frac{\pi\rho gH^2}{4L\sinh 2kd}(\cosh 2ky - 1) \quad (11)$$

In the above equation ρ is the density.

JONSWAP Spectrum

In this study, the dynamic behaviour of the Pelamis WEC under the influence of irregular waves was also analyzed. For this purpose, the JONSWAP spectrum was used for modelling the water levels.

This spectrum was obtained by Hasselmann et al. [1973] during JONSWAP. The equation of this spectrum, which is presented for a wave condition with finite fetch, was modified by Pierson and Moskowitz [1964] spectrum and equation as follows:

$$s(f) = \frac{\alpha g^2}{(2\pi)^4} f^{-5} e^{-1.25\left(f_p/f\right)^4} \gamma^{e^{-\left[\frac{(f-f_p)^2}{2\sigma^2 f_p^2}\right]}} \quad (12)$$

wherein:

$$\gamma = \begin{cases} 5, \text{for } \frac{T_p}{\sqrt{H_s}} \le 3.6 \\ \exp\left(5.75 - 1.15\frac{T_p}{\sqrt{H_s}}\right), \text{for } 3.6 < \frac{T_p}{\sqrt{H_s}} < 5 \\ 1, \text{for } \frac{T_p}{\sqrt{H_s}} \ge 5 \end{cases} \quad (13)$$

$$\sigma = \begin{cases} 0.07, f < f_p \\ 0.09, f < f_p \end{cases} \quad (14)$$

$$\alpha = 0.076\left(\frac{gF}{W^2}\right)^{-0.22} \text{ or } \alpha = 0.0081 \quad (15)$$

$$f_p = \frac{3.5g}{W}\left(\frac{gF}{W^2}\right)^{-0.33} \quad (16)$$

To make this spectrum easier, Hasselmann et al. proposed values between 1.6 and 7 for the coefficient γ, but they recommend 3.3 for general use.

Table 1: Parameters of the wave components for the first series of simulations.

Test case	Wave Amplitude, A (m)	A/a (a, radius of the cylinder)	A' = (A/D) (D, diameter of the cylinder)
1	0.010	0.2	0.10
2	0.015	0.3	0.15
3	0.020	0.4	0.20
4	0.030	0.6	0.30
5	0.040	0.8	0.40
6	0.050	1.0	0.50

Table 2: Parameters of the wave components for the first series of simulations.

Test case	Frequency (Hz)	Wavelength, L (m)	Ka (K, wave number a, radius of the cylinder)
7	0.6	3.458	0.0908
8	0.8	2.270	0.1384
9	1.0	1.539	0.2041
10	1.2	1.081	0.2903
11	1.4	0.796	0.3942

VALIDATION AND RESULTS

Verification of Simulation using AQWA

Loh et al. [2018] predicted and analyzed the behaviour of a horizontal semi-immersed cylinder under various wave conditions using OpenFOAM software that solves Navier-Stokes equations by finite volume method. As they mentioned, it can be considered a simplified model of Pelamis's segments. In their study, they simulated a fixed horizontal semi-submersible cylinder in a numerical tank that was subjected to waves in one side. Then they calculated vertical and horizontal forces applied to the cylinder using the pressure and shear stress data. They compared their result with the forces obtained from the potential theory and the experimental results of Martin and Dixon [1983]. In this paper, to validate the ANSYS AQWA simulation, those data and information were used. Two different series of test cases were performed to estimate the horizontal forces F_x and vertical forces F_y on the horizontal cylinder with a radius of 0.05 m and length of 0.295 m with its centre at the water level. In Table 1, the characteristics of the first series of simulations (1-6) subjected to incident waves with various amplitude and frequencies of 1 Hz and 1.539 wavelength are listed and in Table 2 the second series of simulation (7-11) subjected to incident wave with a constant wave amplitude of 0.02 m and various wavelengths and frequencies are listed.

To simulate a semi-submersible horizontal cylinder in the AQWA software, a surface body was used which was fixed in a numerical tank with 20 m length and 0.6 depth. The density of water was 1,000 kg/m^3. Quadrilateral mesh was generated using specific tools in AQWA where the biggest size of element is 0.004 m and the total number of elements and nodes are 19,624 and 19,626, respectively. In the frequency analysis domain, the frequency range is from 0.1 to 2 Hz with steps of 0.05 Hz. In time analysis domain, the total simulation time is set to 50 starting from 0 and the time step was considered 0.01s.

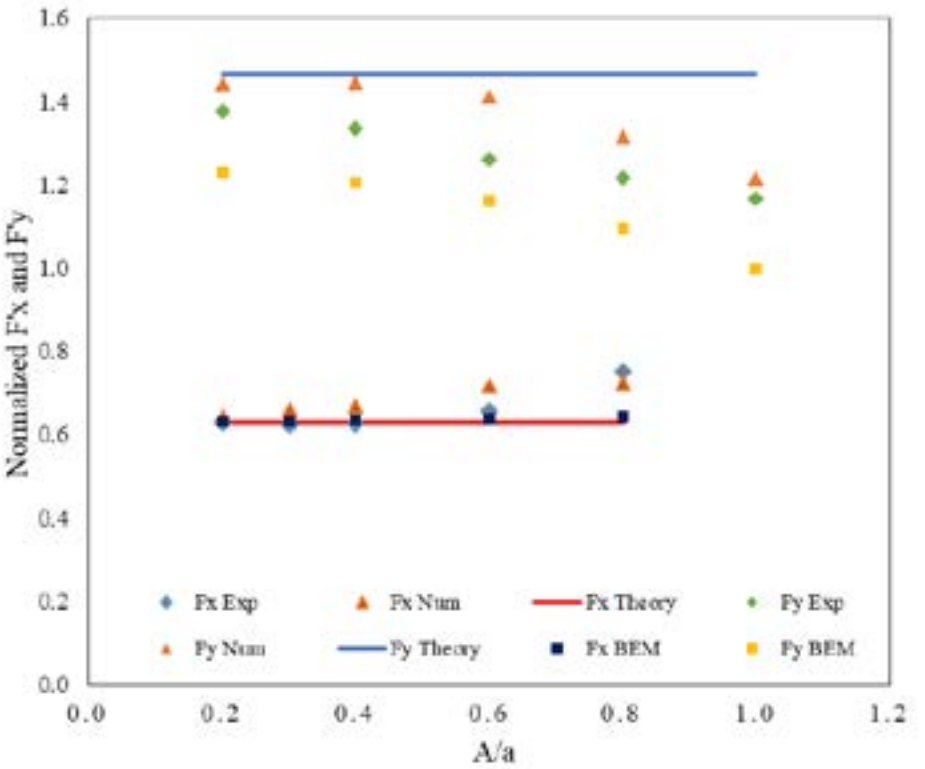

Figure 1: Comparison of the normalized forces in the numerical results, the potential theory, and experimental data of Martin and Dixon [1983].

In order to compare the obtained horizontal forces F_x and the vertical forces F_y with experimental and theoretical results, square root of mean square forces F_{RMS} is calculated using the following equation:

$$F_{RMS} = \sqrt{\frac{1}{T}\int_0^T f(t)^2 dt} \quad (17)$$

where $f(t)$ is the horizontal or vertical forces as a function of time. The numerical force range is calculated based on the root mean square, with the following equation:

$$F_{x,y} = \sqrt{2} \times F_{RMS} \quad (18)$$

To reach the goal of comparability, the dimensionless value of the numerical forces $F'_{x,y}$ are obtained by the following equation:

$$F'_{x,y} = \frac{F_{x,y}}{\rho g a A l} \quad (19)$$

where ρ is the density of water, g is the gravitational acceleration, a is the radius of the cylinder, A is the wave amplitude, and l is the length of the cylinder.

Figure 1 shows the results of solving the governing equation by using the boundary element method and AQWA software, experimental results by Martin and Dixon [1983], theoretical estimates, and also results of finite volume method for the first set of simulations (1-6). There is a good correspondence between the theoretical predictions, the experimental data, and both numerical methods (boundary element and finite volume). The difference between the theoretical estimates and the numerical results

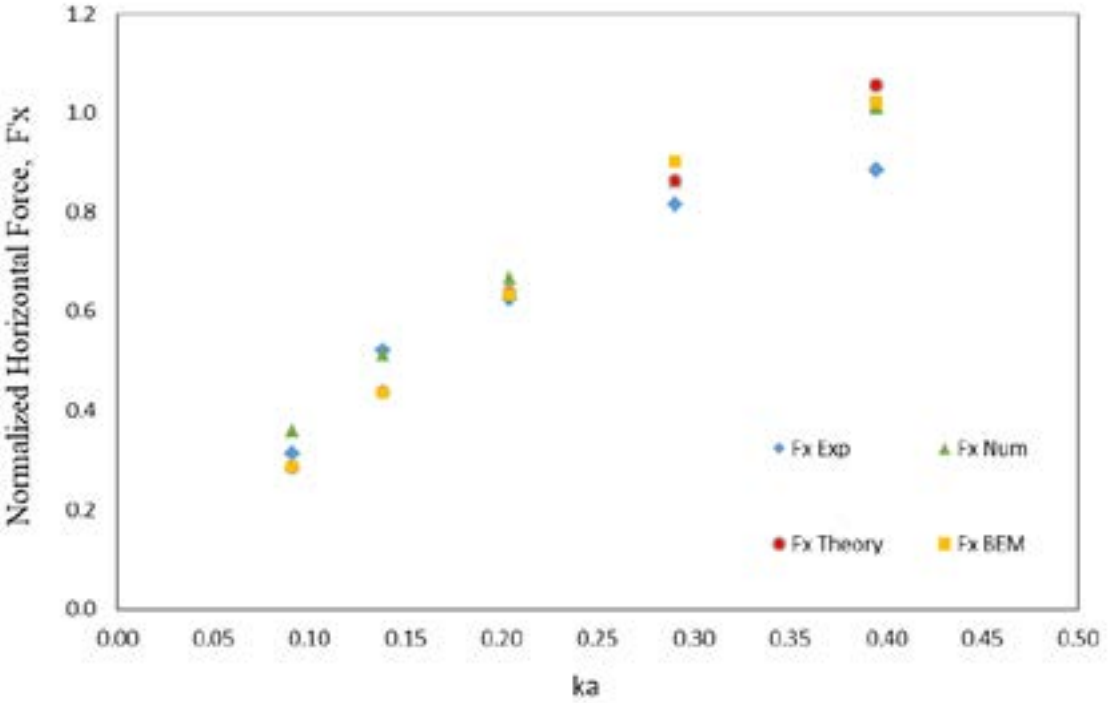

Figure 2: Comparison of the normalized forces F'x and F'y in the numerical simulations, the potential theory, and the experimental data of Martin and Dixon [1983] for simulations (7-11) based on ka.

for the normalized horizontal F'_x and vertical forces F'_y increases with the increasing of A/a, being difference smaller in the horizontal forces F'_x than in the vertical forces F'_y. Similar trends between experimental data and theoretical estimates can also be seen.

Difference for large A/a values is most likely due to nonlinear effects because linear theory is valid only for small A/a values. Based on Martin and Dixon, linear potential theory provides a good estimate for their experimental horizontal forces F'_x, but for vertical forces F'_y it is less accurate when values of A/a are small. In AQWA, the numerical F'_y and experimental F'_y, when A/a=1, have a difference of about 14% and for A/a=0.8, 0.6, 0.4, 0.2 is slightly less than 10%. Numerical F'_x and experimental F'_x have a difference of about 3% when A/a=0.6 and for A/a= 0.4, 0.3, 0.2, it is about 1%. In OpenFOAM, the difference between numerical F'_y and experimental F'_y is about 4% when A/a=0.6; and when A/a=0.4, 0.2, this difference is 1%. The difference between numerical F'_x and experimental F'_x is about 6% when A/a =0.4 and when A/a=0.3 it is about 5% and for A/a=0.2 it is 2%. Generally, the numerical results of the boundary element are in better agreement with the experimental data than theoretical estimates. But the results of the finite volume method are in better agreement with the theoretical estimates. In larger A/a values, the numerical results for both the horizontal and vertical forces and experimental results follow similar trends.

In Figure 2, a comparison between the theoretical estimates, the experimental data, and the numerical results for the second series of simulations (7-11) are presented.

The difference between theoretical results and experimental data by Martin and Dixon [1983] when A/a=0.4 in both horizontal and vertical forces increase with increasing ka.

The results of AQWA and OpenFOAM for numerical horizontal force F'_x are closer to theoretical estimates than experimental data. For vertical F'_y force, the AQWA results are in better agreement with experimental results than theoretical ones, whereas OpenFOAM is closer to the theoretical results. The difference between the numerical results and the experimental data may be due to the difference between the methods of wave generation, absorption, and dumping that are used in numerical methods and physical wave tanks. According to Martin and Dixon [1983], reflection of waves in the experimental study was more than 5%, whereas in AQWA the waves are absorbed along the numerical tank boundaries completely.

Numerical Simulation and Numerical Analysis Results

Computational Space Characteristics

For simulation in AQWA, a numerical tank with a length of 720 m (in y direction) and a width of 120 m (in x direction) and 50 m depth was used. The density of water is 1,025 kg/m^3.

The P2 Pelamis WEC is similar to an eel in a semi-submersible state and has five sections linked by four hinged joints. Each section is 34 m long and weighs 260,000 kg. Pelamis has a total weight of 1,300 tons [Yemm et al., 2012]. The mass of each section is defined and concentrated in its centre of gravity. Other important points in the simulation of the Pelamis is the definition of the moment of inertia with respect to the coordinate system and the water level for Pelamis. An auxiliary tool of ANSYS was used to calculate the depth of Pelamis under the water level and inertia moments, which provides these values based on geometry and structural weight in the form of a default weight. Figure 3 shows the overview of the Pelamis.

For analyzing the effect of different marine conditions on the dynamic behaviour of Pelamis, a set of parameters affecting its behaviour is investigated. In the first case, regular waves are used for dynamic simulation and the parameters like wave height, period, water depth, and angle of incident wave were investigated. In the second case, irregular waves are modelled using the JONSWAP spectrum, the results in this case being compared with regular wave results.

Sensitivity to Meshing

In order to understand the effect of meshing on the numerical solution results, six meshing models, with various number of elements and fine and coarse mesh dimensions, under a wave with amplitude of 1 m and period of 8 s along the longitudinal direction of Pelamis were examined and the vertical forces applied to part 1, the vertical forces applied to joint 1, and the vertical displacement of part 1 in different models of meshing at different times (0 to 50 s) were calculated.

Based on very low effect of meshing dimensions on the boundary element solution and the results in AQWA software, the meshing with 0.5×0.5 dimensions can be used to analyze the hydrodynamic behaviour

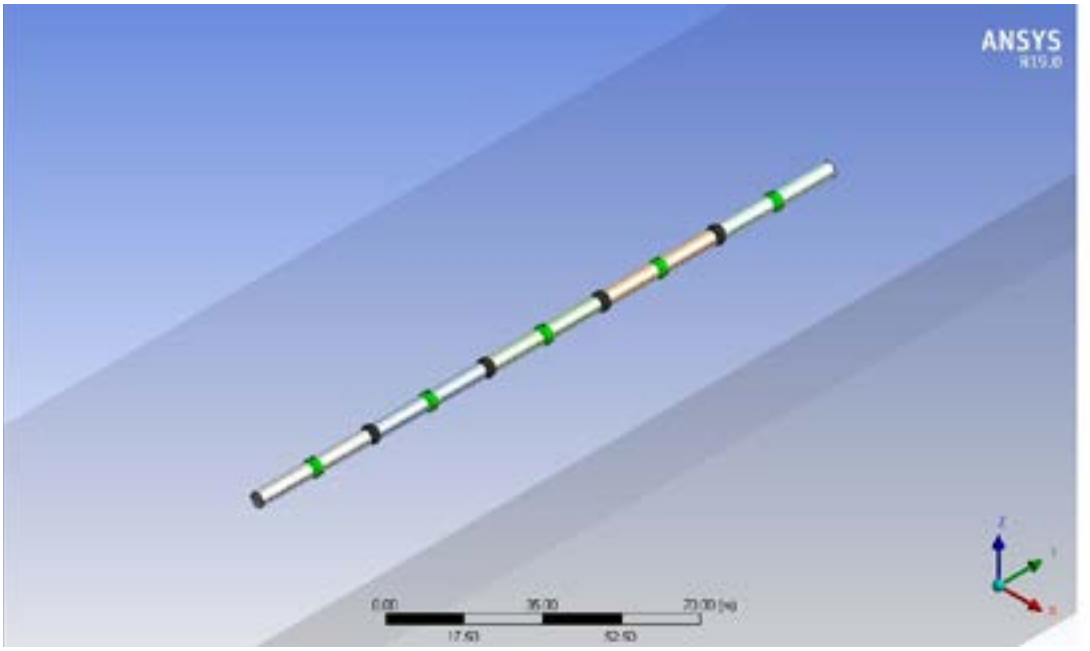

Figure 3: Overview of the Pelamis simulation in AQWA software.

of Pelamis. The other factor affecting the numerical solution is the time step which is considered for analysis. This parameter in the software is determined by the amount of numerical error occurring at each time step of the solution (Time Step Error). However, in all cases, a time step of less than 0.01 s is selected and the numerical error in the time solution is less than $1e^{-10}$.

Sensitivity to Water Depth

Five models of Pelamis (D1 to D5) at different water depths – namely 40, 60, 80, 100, and 1,000 m – were simulated and subjected to a wave with the amplitude of 1 m and a period of 8 s in the longitudinal direction of the Pelamis (y direction) to find the effect of change in water depth. As mentioned previously, the Pelamis WEC is more practical in areas with more than 50 m of water depth; therefore, lower depths were not investigated. To analyze the simulations, the vertical forces applied to part 1, part 2, joint 1, and vertical displacement of part 1 and part 2 were used. In Table 3, the normalized vertical forces F'_y affecting element 1 and joint 1 (connecting element 1 to element 2) at different water depths are reported. We can see that vertical forces acting on part 1 increase with increasing depth, while the vertical forces affecting joint 1 decrease with increasing water depth. Also, there is a sudden change in the numerical forces from D1 to D2 models; this jump from D1 to D2 is clear, while in other cases the changes are not as noticeable. A similar trend is observed in the force acting on joint 1, where the force from the models D1 to D2 abruptly reduces. Therefore, to investigate the cause of this phenomenon, the time series of vertical displacements of part 1 and part 2 in the models D1 and D2 have been normalized and compared. The difference of normalized vertical displacements of part 1 and part 2 are shown in Figure 4. The force

Table 3: Comparing the results of the normalized vertical forces applied to part 1 and joint 1 at different water depths.

Model ID	Water depth (m)	Normalized vertical forces F'_y	
		Part 1	Joint 1
D1	40	0.11742	0.09688
D2	60	0.11847	0.09337
D3	80	0.11863	0.09314
D4	100	0.11865	0.09312
D5	1000	0.11866	0.09311

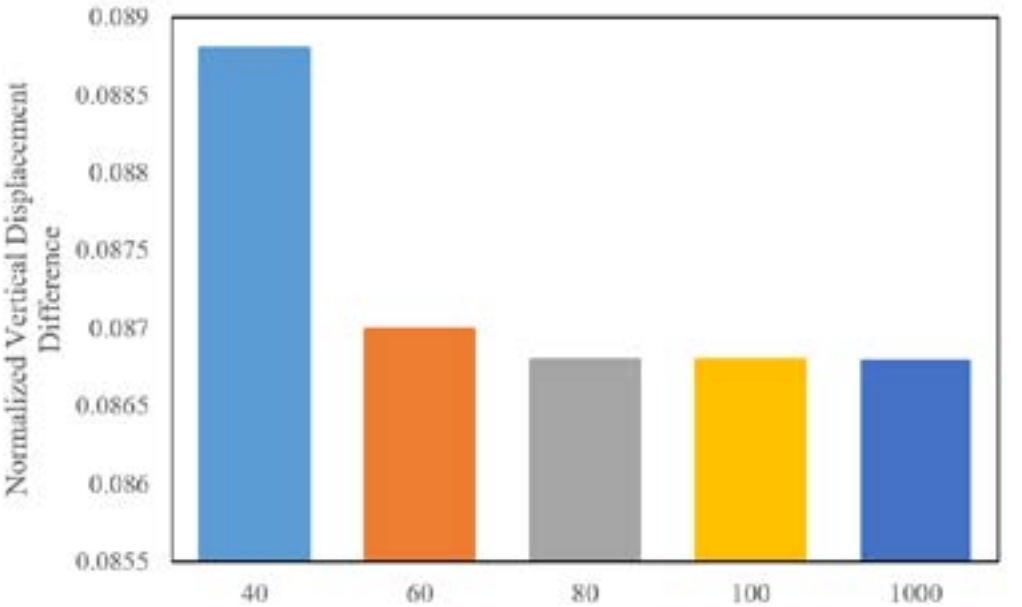

Figure 4: Comparison of the normalized vertical displacement difference for part 1 and part 2 at different water depths.

generated at the junction point is due to the relative displacement of the elements that are connected to it; therefore, according to information in Table 4 and Figure 5, the higher the difference in normalized vertical displacements of part 1 and part 2, the higher the generated force in joint 1, which is also supported by the given information; as it can be seen, the largest difference in normalized vertical displacements occurred at a water depth of 40 m. Therefore, the maximum force created at the joint 1 is in 40 m water depth and with increasing the depth to 60 m, the value of these displacements difference decreases suddenly but as the water depth increases the speed of this difference decreases.

In Figure 6, the normalized vertical forces applied to part 1 at different water depths are compared. It can be seen that the forces increase with increasing water depth and the changes are more severe from D1 to D2, but these differences become lower from D3 model to D5. This difference is because waves with the period of 8 s in water depth of 40 m are in an intermediate zone and they have a wavelength of 98.7 m. With increasing to a water depth of 60 m,

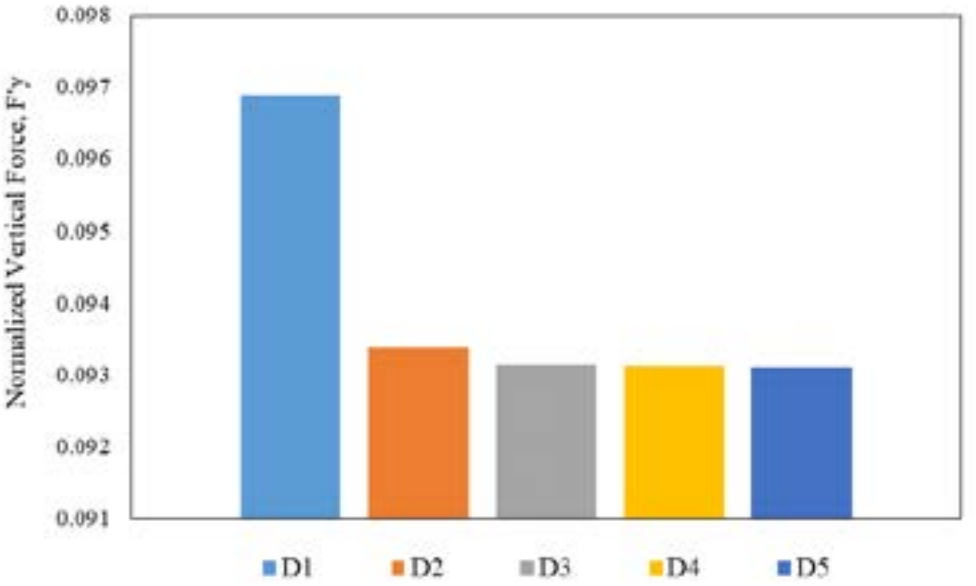

Figure 5: Comparison of the normalized vertical generated forces F'y at joint 1 in different water depths.

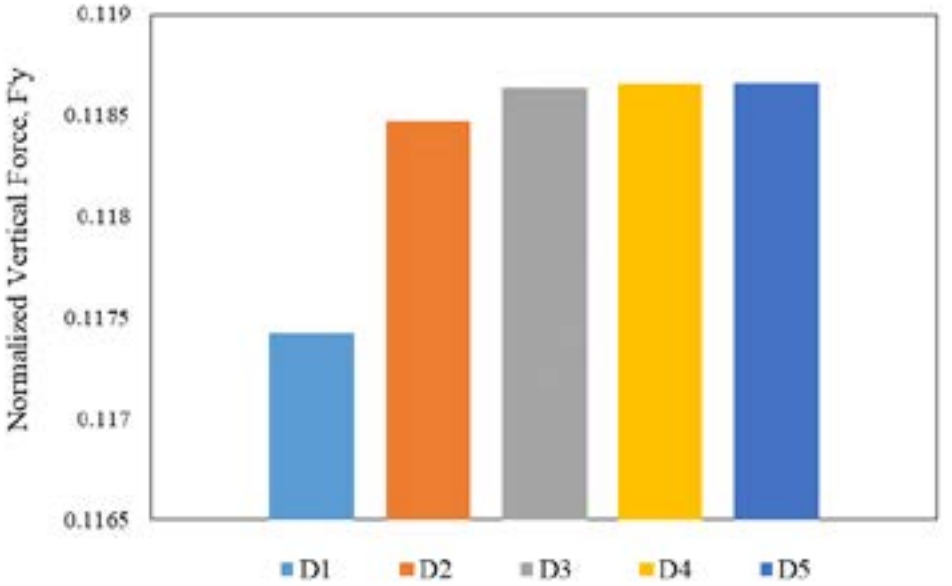

Figure 6: Comparison of the normalized vertical forces F'y applied to part 1 at different depths.

Table 4: Comparison of the results of normalized vertical displacements part 1 and part 2 for different water depth.

Normalized Displacement	Water depth (m)				
	40	60	80	100	1000
Part 1	0.78452	0.78623	0.78707	0.78716	0.78722
Part 2	0.69573	0.69923	0.70030	0.70040	0.70043
Difference	0.0888	0.0870	0.0868	0.0868	0.0868

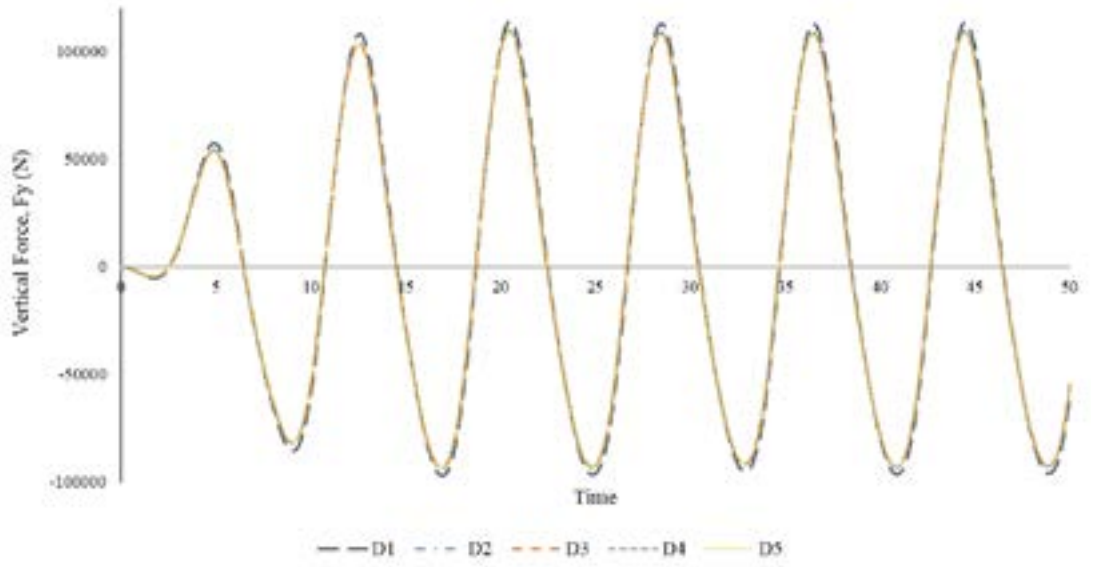

Figure 7: Vertical forces time series for different water depths.

the wave enters the deep water zone and its wavelength becomes equal to 99.9 m and, based on the linear wave theory, increasing wavelength causes increasing wave energy ($E = 0.125 \times \rho \times g \times H2 \times L$) and this increases the force applied to the elements. The increasing in water depth will no longer have a significant effect on the applied forces to the members, since the wavelength in the deep water range will not change significantly.

Figure 7 shows the time series of vertical forces applied to joint 1 at different water depths. In this diagram, the maximum generated force at joint 1 is in D1 model. In Pelamis, the conversion of mechanical energy to electrical energy is done by pumps, which are embedded in the joints; therefore, the greater the generated force in joints, then the more electricity will be produced. Therefore, the D1 model is the most optimal model for generating electricity in terms of the impact of the water depth parameter.

Sensitivity to the Wave Amplitude

Four models (A1 to A4) of Pelamis were simulated and studied under waves with amplitudes of 1, 2, 3, and 4 m, period of 8 s in the longitudinal direction (in the y direction), and in a water depth of 60 m. Table 5 presents the normalized vertical forces F'_y affecting element 1 and joint 1 by waves with different amplitudes. As the wave amplitude increases, the vertical forces F'_y affecting part 1 also increase. The applied F'_y forces to joint 1 also increase with increasing amplitude but, as it can be seen in Figure 8, the acceleration is smaller than the one of part 1. This means that, although the force applied to the joints increases and it increases the produced electricity, this generally indicates a lower efficiency of the device under larger waves. In addition, higher force is created on the bridle cable and a more resistant body is required for the Pelamis to resist under the wave. Therefore, in contrast to our expectations, although larger waves will increase the produced electricity, it does not necessarily mean they increase energy efficiency.

Figure 9 shows the vertical forces time series acting on part 1 due to the waves

Table 5: Comparison of the results of vertical generated forces at part 1 and joint 1 under different wave amplitudes.

Model ID	Wave amplitude (m)	Vertical forces range F_y (kN)	
		Part 1	Joint 1
A1	1	117.9	92.9
A2	2	242.2	187.7
A3	3	375.1	282.7
A4	4	523.0	375.6

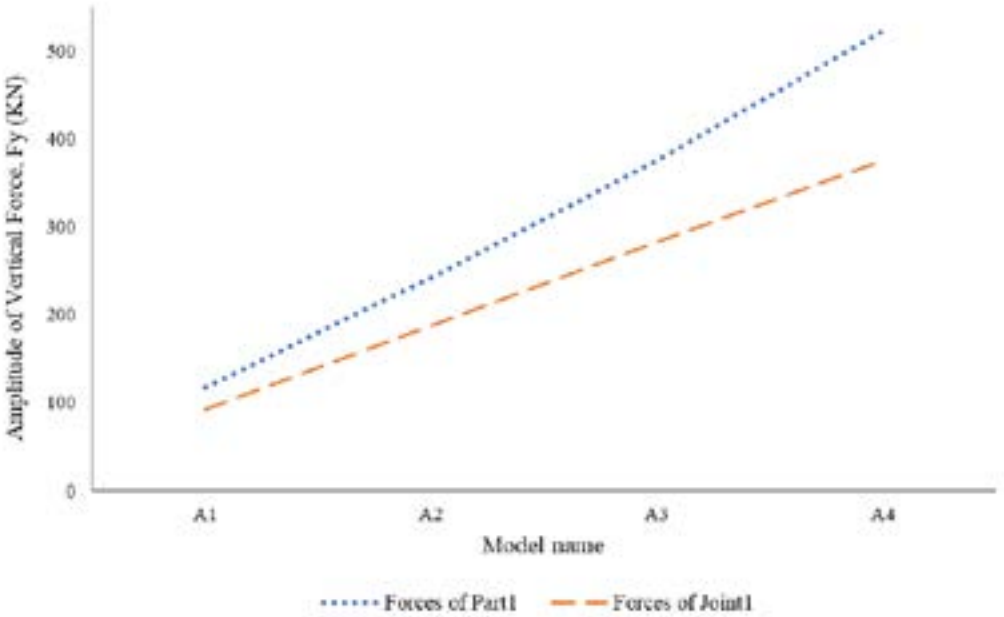

Figure 8: Comparison of the vertical generated forces at part 1 and joint 1 under different wave amplitudes.

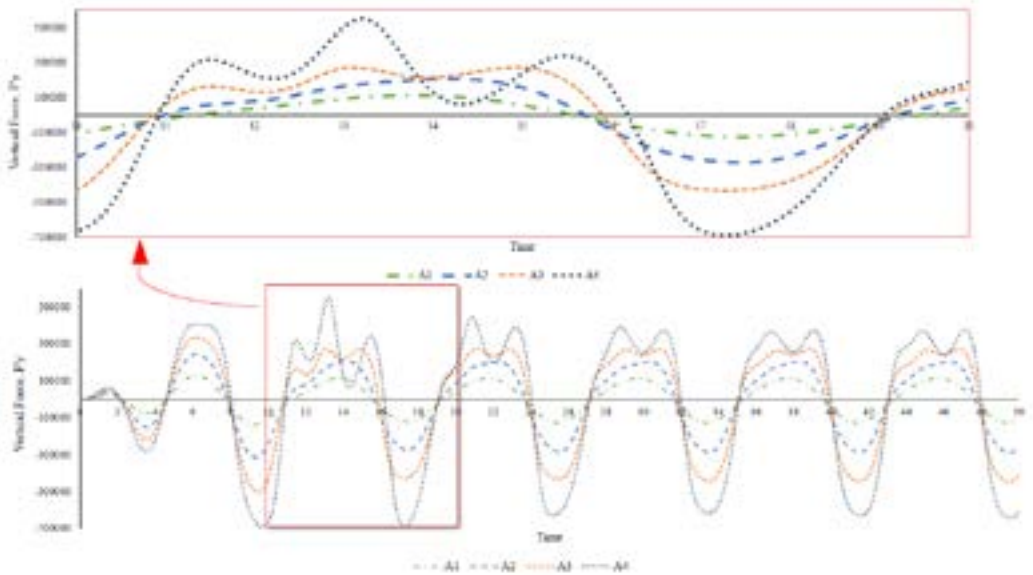

Figure 9: Time series of vertical forces acting on part 1 under waves with different amplitudes.

with different amplitudes. The applied force to element 1 increases with increasing the amplitude wave. The most important point in this graph is the periodicity (period) of the time series of forces which, like the wave period in all models, is approximately 8 s with the exception of the beginning of the graph. This means that the repetition pattern of the forces is similar to the wave surface alignment pattern and the pattern of vertical acceleration of the wave, because, according to the theory of short amplitude waves, the highest vertical applied force by the wave will occur at the moment of maximum vertical acceleration of the wave. According to the amplified part of the graph, which shows time between 10 s to 20 s of simulation, time series in models A1 and A2 have positive max and negative max, but in time series of A3 and A4 models more crests occurred in the positive forces. It was noted previously that the velocity potential function of a problem, based on the superposition principle, is equal to the sum of the velocity potentials of the initial incoming wave, the created wave by the motion of body at six DOF, and the scattered wave due to the presence of a fixed structure. It is obvious that the smaller the amplitude of the wave, the smaller the wave due to its scattering; and the smaller the wave, the less oscillations in the structure in which it has interacted, and the created wave due to this oscillation will be smaller. Therefore, the reason of extra crests in forces time series of models A3 and A4 can be due to this point that amplitude of scattered wave and waves due to the oscillating of the structure increases with the increasing of the wave amplitude and their forces become more visible.

Sensitivity to the Wave Period

Five models (P1 to P5) of Pelamis were studied under the waves in the longitudinal direction (in the y direction) with amplitude of 2 m and periods of 6, 8, 10, 12, and 15 s for the water depth of 60 m.

In Table 6, the numerical results of vertical forces with different periods applied to the element 1 and joint 1 are compared. In model P1 both forces applied to part 1 and joint 1 are maximum compared to the other models, and these forces decrease with increasing periods. In Figure 10 these forces are shown graphically. Based on this figure, the variation of forces which affects part 1 has changed from P2 model onwards and has decreased. A similar trend has occurred for the graph of forces affecting joint 1 in the P3 model and its variation has decreased. According to the finite amplitude wave theory equations for Stokes waves, the greater the wave period, the longer the wavelength and, consequently, it leads to increasing wave energy. In the P1 model, the wavelength is about 56.2 m and the wave power (wave energy per unit time P = nE/T) is 23 kW, while in the P5 model, the wavelength is 351.3 m and the wave power is 69 kW. However, the information presented in this section shows the opposite trend. This means that, despite higher wave energy at greater periods, the Pelamis behaves in a way that creates less forces at its joint points and, consequently, converts less energy. The fact that P2 Pelamis absorbs less energy in longer periods may be due to its length which has not being designed for long waves (as a result of which is not mentioned in this study: the longer the Pelamis's interconnecting segment's length, the better it performs in higher waves). The definition of an optimal model will correspond to the point of the graph with least

Table 6: Comparison of the results of the vertical forces F_y applied on part 1 and joint 1 under waves with different periods.

Model ID	Wave period (s)	Vertical forces range F_y(kN)	
		Part 1	Joint 1
P1	6	437.1	347.9
P2	8	242.2	187.7
P3	10	181.0	54.8
P4	12	134.1	22.6
P5	15	85.8	11.6

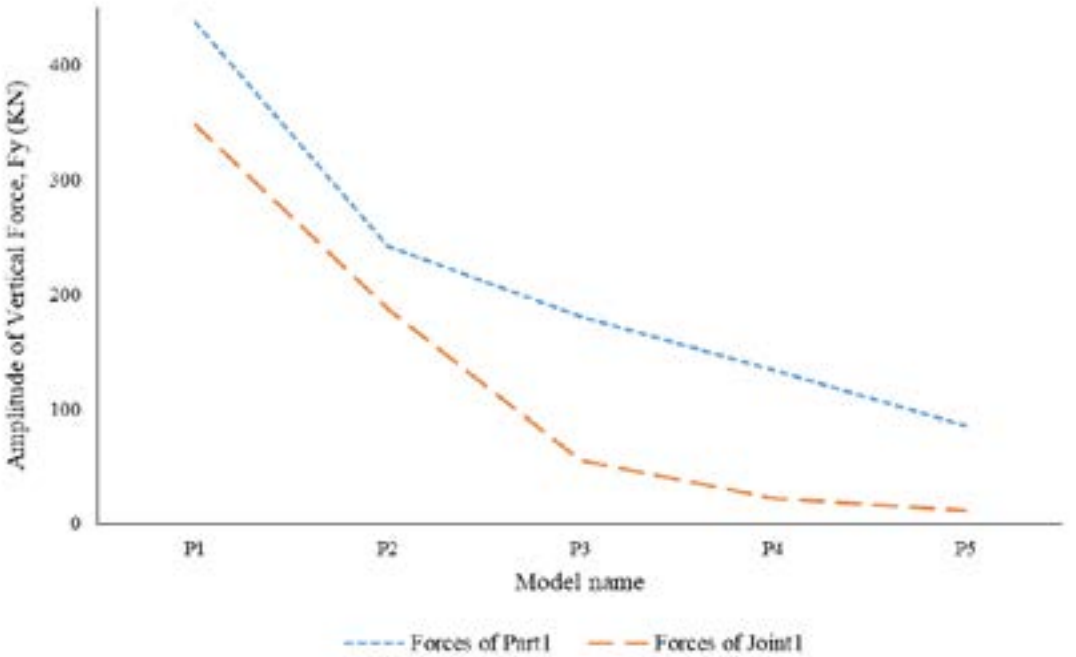

Figure 10: Comparison of the vertical forces applied to part 1 and joint 1 under the effects of waves with different periods.

distance between the force applied to the element and the joint attached to it. According to the diagram, the P2 model, in which the wave period is 8 s, has such a feature and can be considered as the optimal Pelamis device among the simulated models.

In Figure 11, the time series of the vertical forces acting on part 1 under the waves with different periods are shown. In this diagram, except for the transient portion at its beginning, the rest of the periodic time series graph of each force is approximately equal to the corresponding wave period. The important point in this chart is the maximum force applied to the P1 model, which is significantly higher than other models. This has a major impact on the design of the Pelamis's structure and its cables to resist such forces. Another issue is the presence of a secondary crest in the P1 model diagram. These smaller crests may be due to generated waves by the oscillations caused by large wave forces (waves with periods of 6 s in vertical direction that affects element 1 of Pelamis). This effect has not been noticeable in other models.

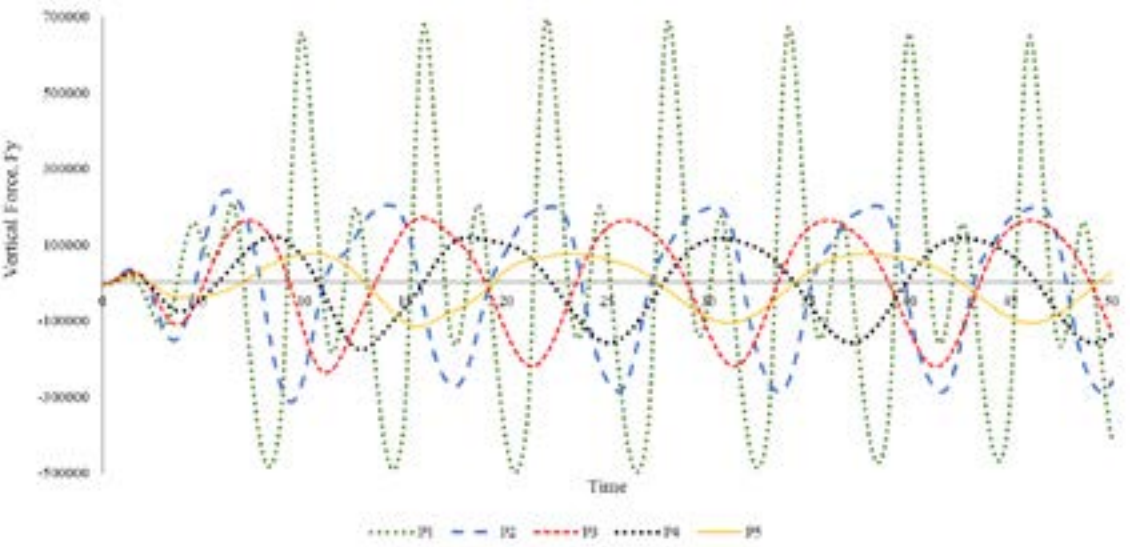

Figure 11: Time series of the vertical forces acting on part 1 under waves with different periods.

Table 7: Comparison of the results of the vertical forces F_y applied to part 1 and joint 1.

Model ID	Wave impact angle (D^0)	Vertical forces range F_y (k N)	
		Part 1	Joint1
Dir1	0	242.2	187.7
Dir 2	30	270.7	116.8
Dir 3	45	293.7	65.7
Dir 4	60	329.8	30.3
Dir 5	90	362.3	11.1

Sensitivity to the Wave Impact Angle

Five models of Pelamis (Dir 1 to Dir 5) are subjected to waves with angles of 0, 30, 45, 60, and 90° to the positive direction of the y-axis with amplitude of 2 m and period of 8 s at a water depth of 60 m. The time-domain solution forces in AQWA are in time series.

Table 7 compares the results of the vertical forces applied to part 1 and joint 1 under the effects of waves with different angles of impact. It can be seen that the more sideways a wave (relative to the longitudinal direction) hits the wave converter, the greater the force is applied to element 1. Since the contact surface of Pelamis along the x-axis is much greater than the contact surface along the y-axis, it is obvious that the closer the wave to the x-axis, the greater the applied force to the surface of the energy converter. The information in Table 7 is plotted in Figure 12. In joint 1, the opposite of part 1, with increasing angle of wave's impact, less force is generated. According to the diagram, this force is almost zero in the Dir 5 model, whereas the maximum force acting on part 1 occurs in this model. This indicates the least energy absorbing function in this case. Based on the above, the best performance is in Dir 1 simulation; the force applied to the elements is minimal while the force generated at the junctions is maximized.

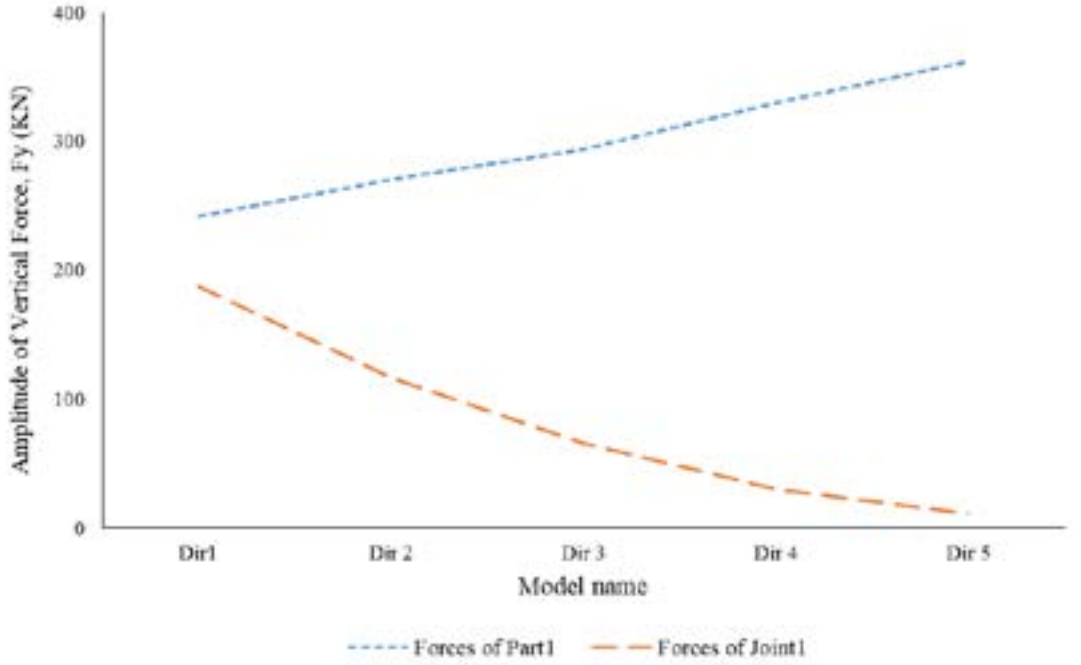

Figure 12: Comparison of vertical forces applied to part 1 and joint 1 under the influence of waves with different angles of impact.

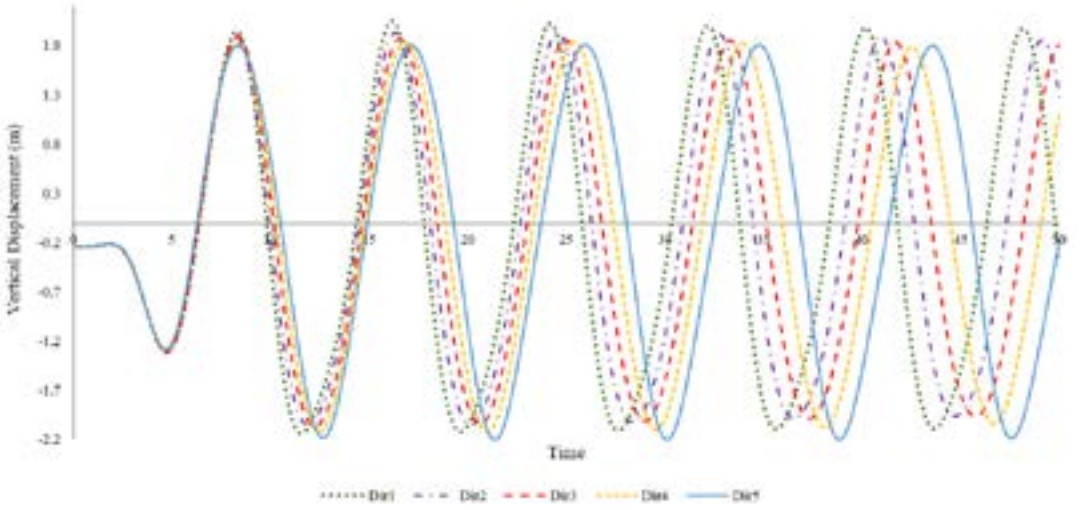

Figure 13: Pelamis vertical displacement time series under impact wave along the x-axis (90^0).

In Figure 13, at the beginning of the diagram, the displacements of all parts of Pelamis are aligned with each other and there will be no force at the joints if there are no relative displacements against each other. Therefore, in Dir 5 model the force acting on the joints is minimized. Over time, the vertical movement phase of the different parts of the Pelamis are slightly different, but the movement phase of the two successive parts, for example part 1 and part 2, against each other is low; that is why the generated force in their joint which connect those parts together reduces. According to what was mentioned, the best performance of the Pelamis WEC occurs in the case where the

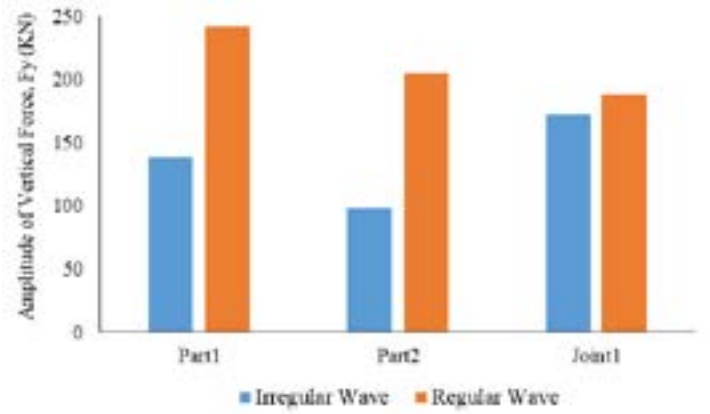

Figure 14: Comparison of the vertical forces on part 1, part 2, and joint 1 under regular and irregular waves.

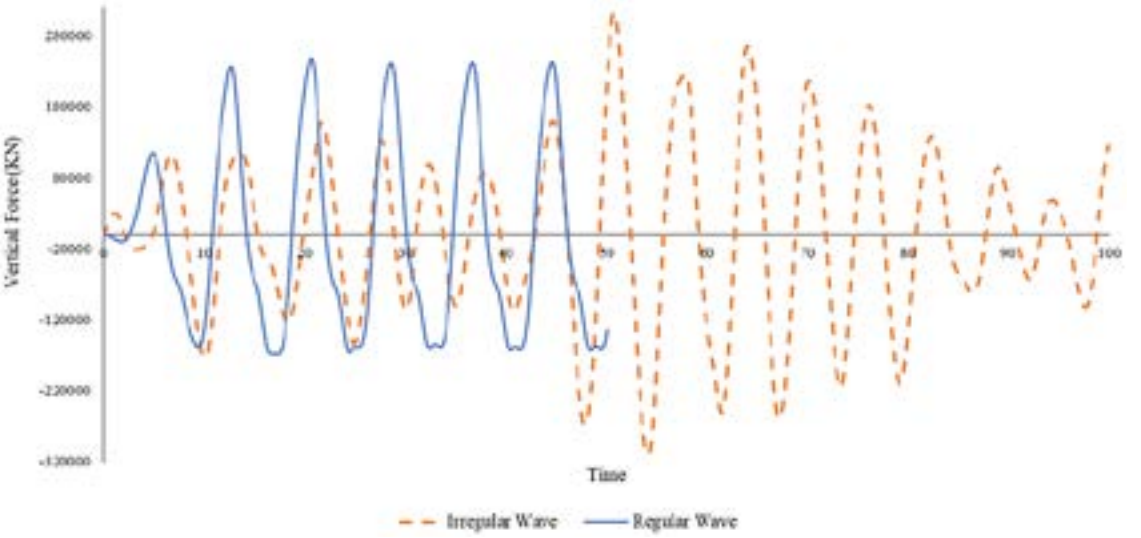

Figure 15: Time series of vertical applied forces to joint 1 under regular and irregular waves.

wave hits in the longitudinal direction of the converter, and the greater this angle, the relative displacements of the segments of the Pelamis will be reduced; therefore, the efficiency of converter will reduce.

Pelamis Behaviour under Irregular Waves

In this section, the Pelamis under the JONSWAP wave spectrum with the wave height of 4 m and period of 8 s at 60 m water depth is simulated. The Gamma in the JONSWAP spectrum was considered equal to 3.3 and the direction of the wave impact is considered along the longitudinal direction of Pelamis (zero degrees relative to the positive direction of the y-axis). The total simulation time was 100 s in order to better observe the irregular effects of waves.

Figure 14 compares the vertical forces F_y on part 1, part 2, and joint 1 under a regular wave with amplitude of 2 m and a period of 8 s at water depth of 60 m and irregular waves which are modelled by the JONSWAP spectrum. The value of applied force to members 1 and 2 reduce significantly with irregular waves. Part 1's force under regular wave was about 240 kN which reduces by 43% to 138 kN under

irregular waves. A similar trend takes place for part 2, where the generated force under regular waves was equal to 205 kN but reduces to 52% and to 98 kN under irregular waves. But this decrease in force due to irregular waves compared to regular waves is only about 8% in joint 1, which indicates a better performance of Pelamis under irregular waves with the JONSWAP spectrum.

In Figure 15, the applied vertical forces to joint 1 are compared in a time series under regular and irregular waves' effects. The regular wave simulation is 50 s long while the irregular wave simulation is set to 100 s, so the blue chart is cut off at 50 s. It can be seen, at the beginning of the simulation, the regular wave forces are greater than the irregular wave forces while, after a certain period of time, the vertical forces increase due to irregular waves. Unlike the irregular wave, the regular wave diagram reaches steady state after approximately 10 seconds and the pattern of diagram changes is repeated afterwards. This is also due to the uniformity of the waves for regular wave.

CONCLUSION

The hydrodynamic conditions of Pelamis's segments and joints under different marine conditions include five models in different water depths, four models with different wave heights, and five models with different periods. Also, five models with different wave impact angles are simulated. Finally, a comparison between the force from regular waves modelled with second-order Stokes wave theory and the irregular waves modelled with the JONSWAP spectrum was made. The results of all these simulations can be summarized as follows:

- In deep water conditions ($d/L>0.5$), increasing or decreasing water depth when other influential parameters are constant will not affect the hydrodynamic performance of P2 Pelamis because the wavelength does not change.
- Outside the deep water range ($d/L\leq0.5$), increase in the water depth due to the increase in the wavelength increases the force applied to the energy converter segments, while this increase in depth decreases the relative displacement of segments and decreases the force applied at joints.
- As the height of the wave increases, when the other factors are constant, the forces applied on Pelamis's segments and joints increase. It should be noted that the forces applied to the segments increase more rapidly than the generated forces in the joints.
- Based on what was mentioned above, increasing the amplitude of waves increases absorbed energy by Pelamis but reduces its operating efficiency.
- Increasing the period of the wave reduces the forces applied to segments and joints of the WEC.
- In terms of performance of the device, the optimal period is 8 s, since the difference between the forces applied to the Pelamis's segments and joints is minimum.
- The closer the wave impact angle of Pelamis to its longitudinal direction, more force is created at its joints and the device performs better. On the other hand, the closer this angle is to the perpendicular angle to the longitudinal axis of Pelamis, the greater the applied force to the segments and the efficiency of the converter approaches to zero.

- The force applied to the segments of P2 Pelamis under the JONSWAP irregular wave spectrum is less than the force generated at its joints; however, the forces applied to the segments are always greater than the forces generated in the joints under regular waves. This indicates better performance of the P2 Pelamis under irregular waves.

REFERENCES

Bruinsma, N.; Paulsen, B.T.; and Jacobsen, N.G. [2018]. *Validation and application of a fully nonlinear numerical wave tank for simulating floating offshore wind turbines*. Ocean Engineering, 147:647-658.

Dalton, G.J.; Alcorn, R.; and Lewis, T. [2010]. *Case study feasibility analysis of the Pelamis wave energy convertor in Ireland, Portugal and North America*. Renewable Energy, 35 (2):443-455.

Gaffney, O. and Steffen, W. [2017]. *The anthropocene equation*. The Anthropocene Review, 4 (1):53-61.

Ganesan, T.S. and Sen, D. [2015]. *Time-domain simulation of large-amplitude wave–structure interactions by a 3D numerical tank approach*. Journal of Ocean Engineering and Marine Energy, 1 (3):299-324.

Hasselmann, K.F.; Barnett, T.P.; Bouws, E.; Carlson, H.; Cartwright, D.E.; Eake, K.; Euring, J.A.; Gicnapp, A.; Hasselmann, D.E.; and Kruseman, P. [1973]. *Measurements of wind-wave growth and swell decay during the Joint North Sea Wave Project (JONSWAP)*. Ergaenzungsheft zur Deutschen Hydrographischen Zeitschrift, Reihe A.

Huntley, D.A. [1977]. LE MÉHAUTÉ, B. *An introduction to hydrodynamics and water waves*. Springer-Verlag, New York, viii+ 323 p. Wiley Online Library.

Li, Y. and Lin, M. [2012]. *Regular and irregular wave impacts on floating body*. Ocean Engineering, 42:93-101.

Liu, C.F.; Teng, B.; Gou, Y.; and Sun, L. [2011]. *A 3D time-domain method for predicting the wave-induced forces and motions of a floating body*. Ocean Engineering, 38 (17-18):2142-2150.

Liu, Y.; Gou, Y.; Teng, B.; and Yoshida, S. [2016]. *An extremely efficient boundary element method for wave interaction with long cylindrical structures based on free-surface Green's function*. Computation, 4 (3):36.

Loh, T.T.; Pizer, D.; Simmonds, D.; Kyte, A.; and Greaves, D. [2018]. *Simulation and analysis of wave-structure interactions for a semi-immersed horizontal cylinder*. Ocean Engineering, 147:676-689.

Mahmoudi, M. [2021]. *Identifying the main factors of Iran's economic growth using growth accounting framework*. European Journal of Business and Management Research, 6 (5):239-245.

Mahmoudi, M. [2022]. *COVID lessons: was there any way to reduce the negative effect of COVID-19 on the United States economy?* arXiv preprint arXiv:2201.00274.

Mahmoudi, M. and Ghaneei, H. [2022]. *Detection of structural regimes and analyzing the impact of crude oil market on Canadian stock market: Markov Regime-Switching Approach*. Studies in Economics and Finance.

Martin, P.A. and Dixon, A.G. [1983]. *The scattering of regular surface waves by a fixed, half-immersed, circular cylinder*. Applied Ocean Research, 5 (1):13-23.

Pierson Jr., W.J. and Moskowitz, L. [1964]. *A proposed spectral form for fully developed wind seas based on the similarity theory of SA Kitaigorodskii*. Journal of Geophysical Research, 69 (24):5181-5190.

Thomson, R.C.; Chick, J.P.; and Harrison, G.P. [2019]. *An LCA of the Pelamis wave energy converter*. International Journal of Life Cycle Assessment, 24 (1):51-63.

Westphalen, J.; Greaves, D.M.; Hunt-Raby, A.; Williams, C.J.K.; Taylor, P.H.; Hu, Z.Z.; Causon, D.M.; Mingham, C.G.; Stansby, P.K.; and Rogers, B.D. [2010]. *Numerical simulation of wave energy converters using Eulerian and Lagrangian CFD methods*. Twentieth International Offshore and Polar Engineering Conference.

Yemm, R.; Pizer, D.; Retzler, C.; and Henderson, R. [2012]. *Pelamis: experience from concept to connection*. Philosophical Transactions of the Royal Society A: Mathematical, Physical and Engineering Sciences, 370 (1959):365-380.